



Film cooling performance measurement over a flat plate for a single row of holes embedded in an inclined trench

Sanjay D. Barahate^{*}, R.P. Vedula^{**}

Department of Mechanical Engineering, Indian Institute of Technology Bombay, Mumbai, India

ARTICLE INFO

Keywords:

Film cooling
Inclined trench
Effectiveness
Heat transfer

ABSTRACT

Film cooling heat transfer coefficient and effectiveness measurements downstream of a single row of holes embedded in an inclined trench injecting secondary fluid into the mainstream over a flat surface are reported here. The well-studied trench geometry is one where the walls of the trench are perpendicular and film injection holes are at an angle to the mainstream flow direction. In the current investigation, the trench is inclined at an angle to the mainstream and the injection holes are normal to the flow direction. Coolant injection in the form of a uniform stream at an angle to the mainstream is likely with this configuration. The trench inclination is kept constant at 35° and three hole pitch to diameter ratios equal to 3, 4.5 and 6 are studied for the blowing ratio varying between 0.3 and 2.5. The injection hole length to diameter ratios equal to 1.8 and 5.5 were studied and the influence on the net heat flux reduction ratio was found to be very small. The local effectiveness and the heat transfer coefficient values are presented and the variations in the cross-stream direction are observed to be very small. The effectiveness values for the current angular trench are higher whereas the heat transfer coefficients are smaller compared to the normal trench at higher blowing ratios. This results in increased Net Heat Flux Reduction ratio (NHFR) values for the current configuration which are observed to remain high at large downstream locations also.

1. Introduction

Film cooling performance for a flat plate geometry is a well-studied phenomenon and a variety of different hole configurations for film injection into the mainstream have been reported. Film cooling is one of the several methodologies used in keeping the blades of gas turbine engines within permissible temperature limits. The injection of coolant into a trench before it exits into the mainstream is a relatively new concept. Bunker [1] presented a review of different injection geometries including simple cylindrical holes, shaped holes and holes in a trench and reported that the performance of trench geometries is very good at large blowing ratios. It was reported that the trench could be manufactured using the protective coatings that applied to the surface. Lu et al. [2] reported local as well as spanwise averaged effectiveness and heat transfer coefficient values for a row of cylindrical inclined holes embedded in transverse trenches with different trench depths and widths and compared the results with those from shaped hole experiments. The trench depth equal to 0.75d with width equal to 3d was reported to provide the highest averaged film cooling effectiveness, and

while the values were considerably lower than those for shaped holes at low values of blowing ratio (M nearly equal to 0.5), the performance was better for high blowing ratio values (M greater than about 1.5). Khalatov et al. [3] reported averaged effectiveness values in the stream wise direction for coolant injection into transverse shallow trenches with and without mainstream acceleration. The film cooling effectiveness for the trench geometry was reported to be 2 to 3.5 times greater than that for simple cylindrical holes at larger blowing ratio values. Jia et al. [4] reported effectiveness values for a row of holes, with compound angles equal to 0°, 45°, and 90°, embedded in a transverse trench. The film cooling performance was reported to improve with compound angle holes and the highest values were reported for the holes with compound angle equal to 45°. Zuniga and Kapat [5] investigated film cooling performance of cylindrical and shaped holes embedded in a normal trench with P/d equal to 4, 8 and 12. The effectiveness for the cylindrical holes was reported to be higher than that for shaped holes embedded in the trench by about 25–35%. The laterally averaged effectiveness for P/d equal to 4 was reported to be higher compared to P/d equal to 8 and 12.

Lee and Kim [6] reported computational results for film cooling

^{*} Corresponding author.

^{**} Corresponding author.

E-mail addresses: sanjaybarahate@gmail.com (S.D. Barahate), rpv@iitb.ac.in (R.P. Vedula).

Nomenclature

$h(x, y)$	Local heat transfer coefficient at location (x, y) , W/m^2K
$h(x)$	Spanwise averaged heat transfer coefficient at location x , W/m^2K
$h_o(x, y)$	Local heat transfer coefficient without film cooling, W/m^2K
$NHFR(x, y)$	Net Heat Flux Reduction ratio at location (x, y)
$NHFR(x)$	Spanwise averaged Net Heat Flux Reduction ratio at location x
$q(x, y)$	Local heat flux supplied to plate at location (x, y) , W/m^2
$q_f(x, y)$	Local heat flux with film cooling at location (x, y) , W/m^2
$q_o(x, y)$	Local heat flux without film cooling at location (x, y) , W/m^2
q_{loss}	Heat loss from outer surface, W/m^2
$T_{aw}(x, y)$	Adiabatic wall temperature at location (x, y) , K
T_j	Secondary air jet temperature, K
$T_w(x, y)$	Wall temperature at location (x, y) , K
T_∞	Main stream temperature, K
U_∞, U_j	Mainstream and secondary fluid velocity, m/s

Roman Alphabets

A	Area of heated foil, m^2
---	----------------------------

d	Diameter of injection hole, m
D	Projected length of upper surface of trench, m
I	Current, A
L	Length of injection hole, m
M	Blowing ratio, $(\rho_j U_j)/(\rho_\infty U_\infty)$
P	Pitch of injection holes, m
V	Voltage, V
W	Width of trench, m
X	Streamwise distance downstream of the injection hole, m
Y	Spanwise distance, m

Greek Alphabets

α	Angle of injection hole with surface in stream wise direction
δ	Boundary layer thickness, m
δ^*	Displacement thickness, m
$\eta(x, y)$	local effectiveness
$\eta(x)$	Spanwise averaged local effectiveness
η	Overall averaged effectiveness
ρ	Density, kg/m^3
ϕ	Overall cooling effectiveness

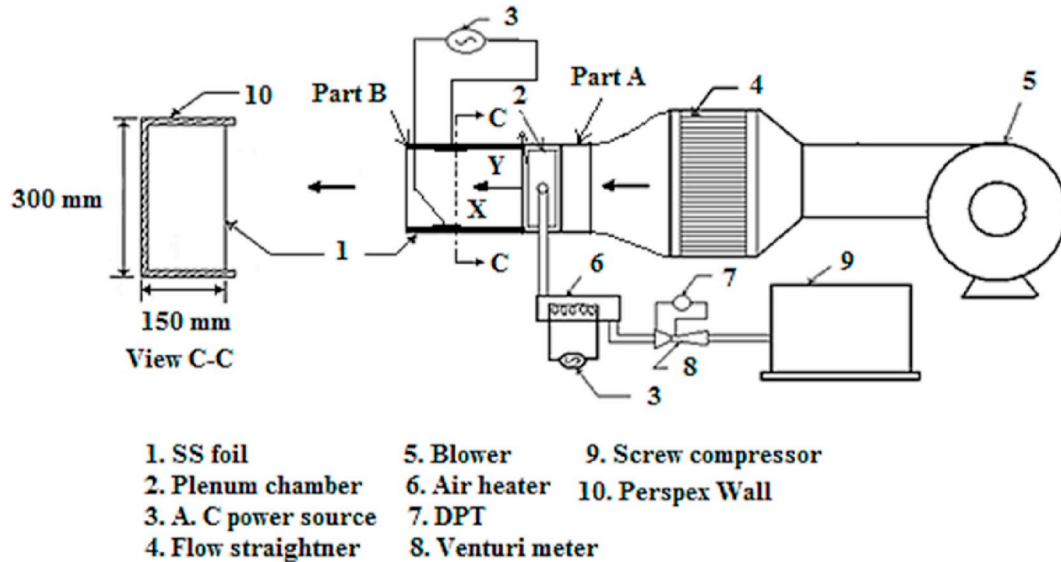


Fig. 1. Schematic of film cooling experimental facility.

effectiveness for a row of holes embedded in a transverse trench. The transverse trench with width equal to two times diameter and height equal to one diameter was reported to result in the best performance at blowing ratio equal to 0.6 and 1.4. Abdala et al. [7] reported computational studies for adiabatic effectiveness for inclined holes injecting into a multi-trench geometry which consisted of a narrow trench in a wide trench and the effectiveness of the multi-trench geometry was reported to be higher than that of the regular trench geometry. Oguntade et al. [8] reported centerline and averaged effectiveness of film cooling for beveled and filleted outlet edge trenches with inclined hole injection. Filleted outlet edge trench holes were reported to produce higher film cooling effectiveness than the beveled and normal trenches. Zhang et al. [9] reported film cooling performance of a single row of holes embedded in a saw-tooth slot (trench) for corner angles equal to 60° , 90° , 120° and 150° and the performance was reported to be highest for the corner

angle equal to 60° . Kianpour et al. [10] investigated film cooling effectiveness for cylindrical and trenched holes normal to the surface of a combustor surface for blowing ratio equal to 1.25 and 3.18 for injection holes inclined at 30° . The trenched holes were reported to have double the effectiveness of the base holes. Pakhamov et al. [11] used the 3D Reynolds averaged Navier-Stokes equations with the Reynolds stress turbulence model to predict the performance of film cooling injection into a trench. High effectiveness values at high blowing ratios was reported and the comparison with experimental data was reported to be satisfactory. Wang et al. [12] reported a numerical study for the influence of uncertainty in four geometric parameters on the film cooling effectiveness for secondary fluid injection into a trench geometry. It was concluded that the fillet radius of the trench trailing corner was the most sensitive parameter. He et al. [13] reported numerical results for trench film cooling over a turbine vane. A shaped trench called the segmented

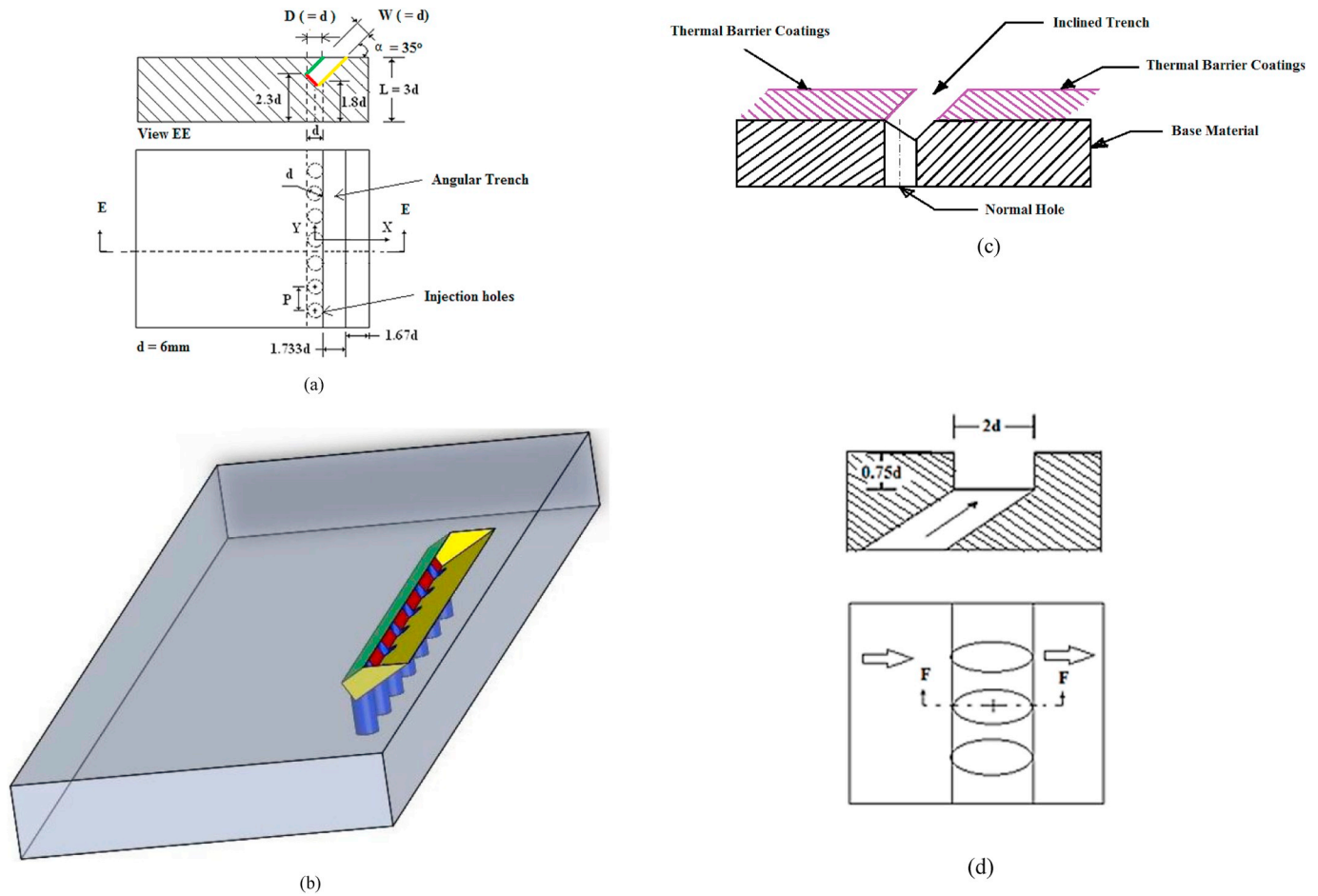


Fig. 2. (a) Injection plate geometry of an inclined trench, (b) isometric view of an inclined trench (c) Inclined trench made by depositing thermal barrier coatings by using parallelepiped mask and (d) injection plate geometry for a normal trench.

Table 1
Details of experimental setup of film cooling.

Sr. No.	Parameter	Value
1.	Diameter of injection hole, d	6 mm
2.	Injection angle, α	35°
3.	Pitch to diameter ratio, P/d ; length to diameter ratio, L/d	3, 4.5 and 6; 1.8 and 5.5
4.	Width to diameter ratio, W/d	1
5.	Main stream velocity, U_∞	33.54 m/s
6.	Temperature of mainstream, T_∞ ; Temperature of injection air, T_j	$30 \pm 2^\circ\text{C}$; $60 \pm 2^\circ\text{C}$
7.	Density ratio, (ρ_j/ρ_∞) and Blowing ratio, M	0.92; 0.3–2.5
8.	Boundary layer thickness to jet diameter ratio, δ/d ; displacement thickness to jet diameter ratio, δ^*/d	0.94; 0.117

trench was proposed and the effectiveness of this geometry was reported to be better in the low curvature portion of the vane.

An advantage of the trench geometry is that it provides smaller span wise variation of the effectiveness and heat transfer coefficients compared to other geometries. This happens due to the physical barrier of the trench wall on which the jets tend to impinge on. Typically, the trench wall is perpendicular and injection holes are inclined to the direction of the mainstream but in this study a modified configuration is proposed where the trench walls are inclined but the injection holes are perpendicular to the mainstream flow. This geometry can be expected to result in the ejection of the coolant in the form of a nearly uniform slot jet into the mainstream at a desired angle, which can be more effectively turned towards the surface than a stream injected normal to the surface.

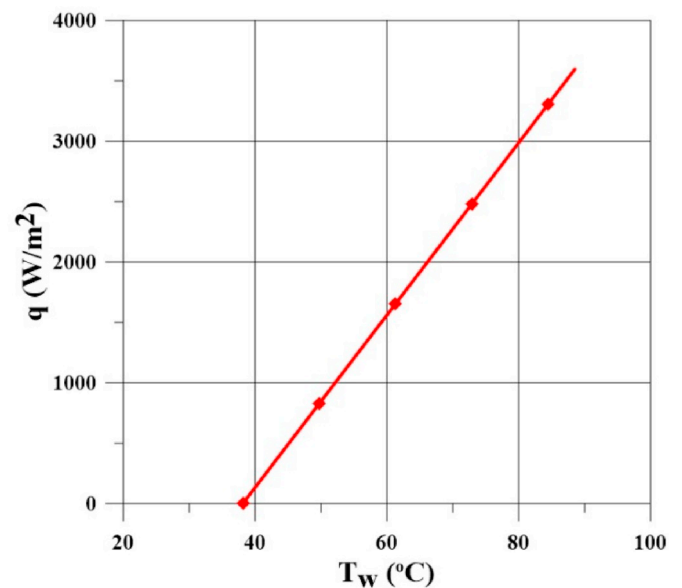


Fig. 3. Plot of heat flux versus wall temperature.

A suggested methodology for the manufacture could be similar to what has been done for the normal trench [1]. The holes are first made on the blade surface and the trench is obtained by using the thermal barrier coating with a suitable masking device. The effectiveness and heat

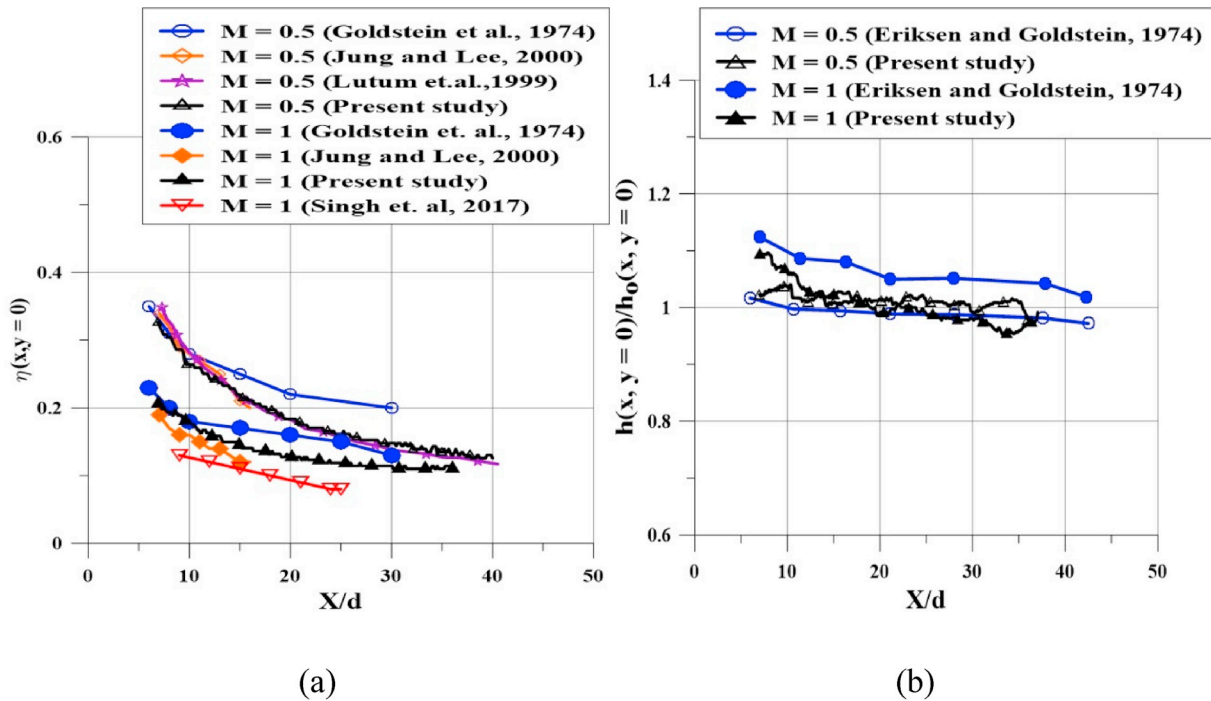


Fig. 4. Comparison of (a) centerline effectiveness and (b) $h(x, y)/h_0(x, y)$ of single row of cylindrical injection holes over a flat plate for $M = 0.5$ and 1 and for $\alpha = 35^\circ$.

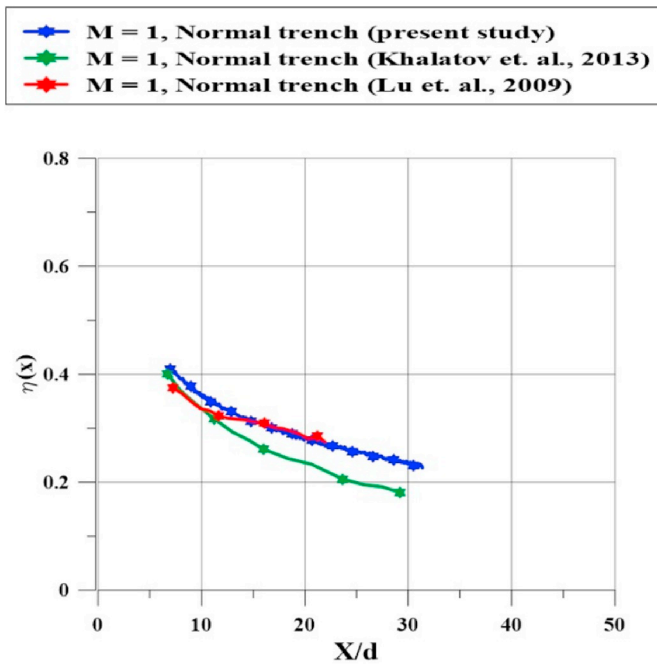


Fig. 5. Comparison of averaged effectiveness of normal trench.

transfer coefficient values for this geometry are reported for several blowing ratio (M) values, length to hole diameter ratio (L/d) values and pitch to hole diameter ratio (P/d) values for a trench with a 35° inclination angle. The results are then compared with geometries for which good film cooling performance has been reported.

2. Experimental setup

A schematic of the experimental setup used in the current

investigation is shown in Fig. 1. A centrifugal blower with a rectangular exit section was used to provide the required air flow rate of the main stream. The exit of the blower was connected to a long rectangular cross section duct and subsequently to serially placed expansion, honeycomb and contraction sections (designed as in Ref. [14], and terminated in a $150 \text{ mm} \times 300 \text{ mm}$ rectangular section. The uniformity of velocity at the exit of this rectangular section was verified by measurements using a pitot tube.

The test section was made in two parts – Part A and Part B, each 350 mm long. Part A was a $150 \text{ mm} \times 300 \text{ mm}$ cross-section rectangular passage with three walls made of 10 mm thick Perspex. The fourth wall also made of Perspex was the injection plate in which the film cooling hole geometries were machined. Part B was also a rectangular cross-section duct with three walls of 10 mm thick Perspex but the fourth wall was made of a 0.15 mm thick stainless steel (SS) foil-wall to obtain an internal cross section of $300 \text{ mm} \times 150 \text{ mm}$ as shown in view CC. One end of the Part A was attached to the rectangular exit section from the blower while the other end was attached to Part B such that the injection plate of Part A and stainless steel foil-wall of Part B were flush with each other. The parts A and B together formed a 700 mm long test section with a $150 \text{ mm} \times 300 \text{ mm}$ cross section area. The stainless steel foil had two thick copper bus bars soldered at the ends which were connected to a high current and low voltage ($I = 500 \text{ A}$, $V = 5 \text{ V}$) AC power supply. One face of the stainless steel foil-wall, exposed to the mainstream and film flows, was kept shiny while the other face exposed to the ambient was painted black to make the emissivity as close to unity as possible. The temperature of the surface of the foil that was painted black was measured by viewing it using a thermal camera (Mikron-M7600PRO). Eight K-type thermocouples were fitted in the test section at the inlet to measure temperature of the mainstream and two K-type thermocouples were provided in the area surrounding the test section, to measure the ambient temperature.

A plenum chamber made of Perspex was fixed to the injection plate for supplying secondary air to the test setup. The secondary air from a screw compressor passed through a venturi meter which had a differential pressure transducer (DPT) connected across the inlet and throat diameters for obtaining the volume flow rate of injected air entering the

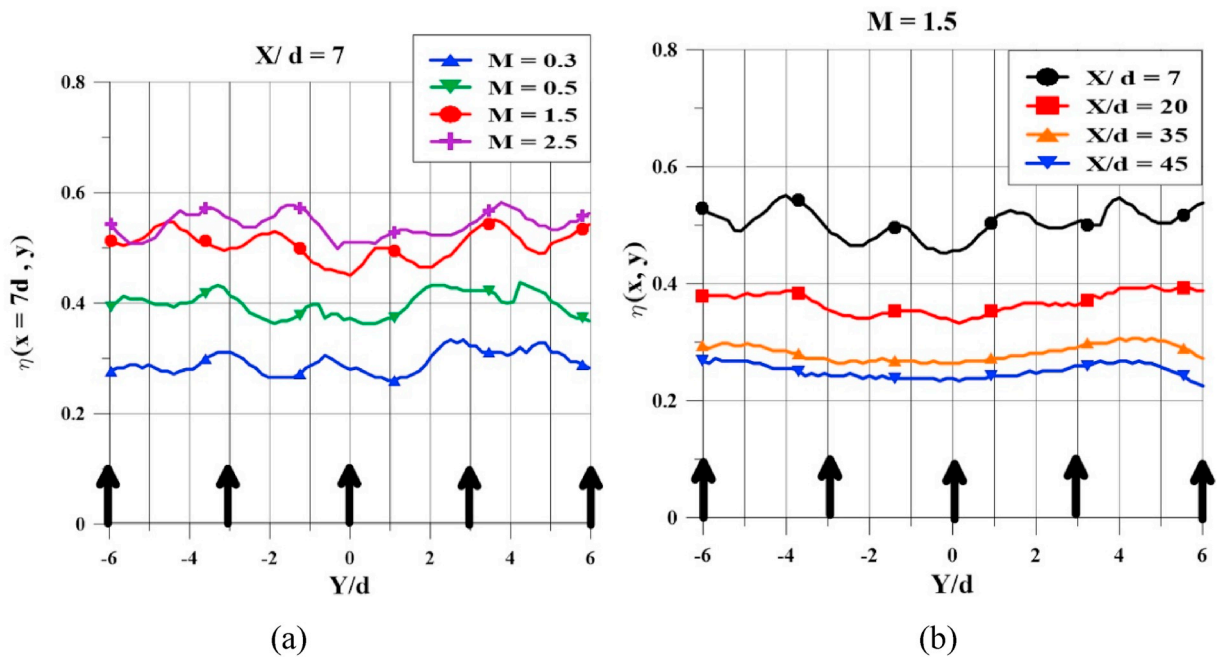


Fig. 6. Distribution of spanwise local effectiveness (a) different blowing ratio (M) at $X/d = 7$ and (b) different X/d for $M = 1.5$.

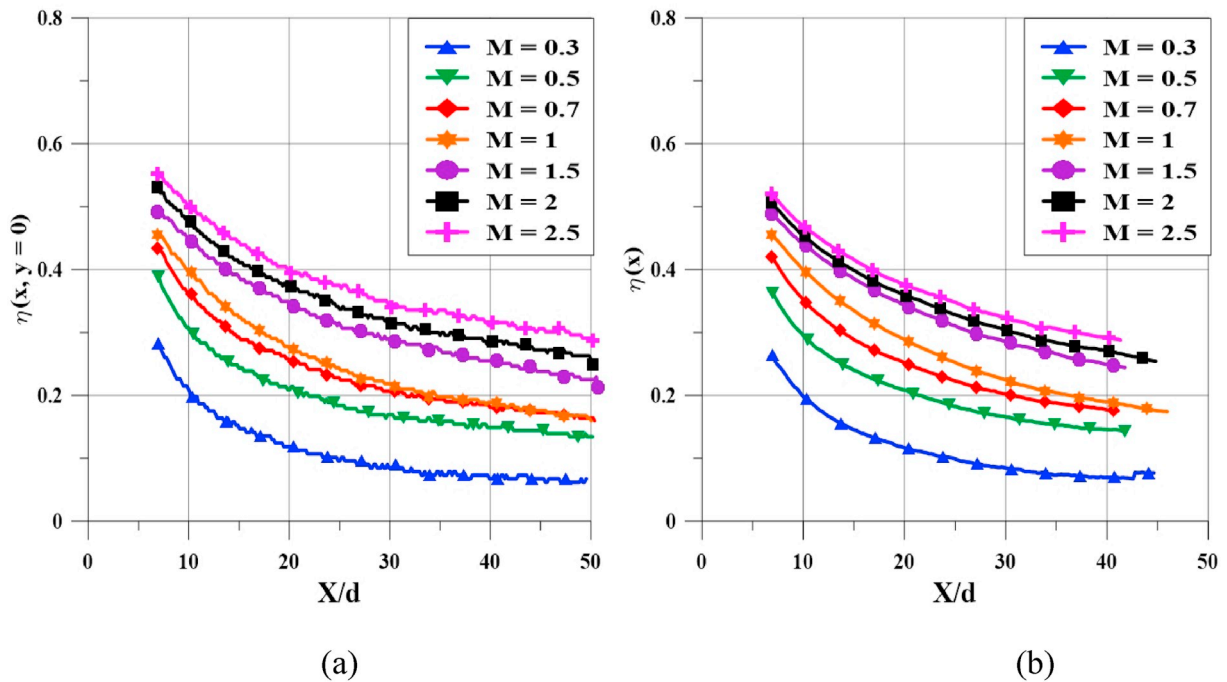


Fig. 7. Distribution of (a) centerline and (b) spanwise averaged effectiveness for different blowing ratio.

plenum chamber. The absolute pressure at the venturi meter throat, measured using a pressure transducer, was used for computing the mass flow rate of injection air. The air then passed through a heater section where it was heated to about 60°C before entering the plenum chamber. K-type thermocouples were fitted in the plenum chamber just upstream of each location where the air entered the holes machined in the injection plate, to measure temperature of the injection air into each hole. Experiments were performed by heating the injected stream instead of the mainstream. However, since the density ratio is very close to unity measurements of effectiveness and non dimensional heat transfer coefficients for film heating and film cooling are equivalent.

An inclined trench at an angle equal to 35° was machined in the injection plate as shown in Fig. 2 (a). The width (W) and depth (D) of the angular trench were defined as the perpendicular distance between the parallel faces and the length along the mainstream direction of the smaller of the two parallel surfaces of the trench respectively. Injection holes were drilled perpendicular to the mainstream direction. The width and depth of the trench were both taken equal to the injection hole diameter (d) in this investigation and therefore the fluid exiting from the injection holes completely impinges on the smaller face of the angled trench. There are several geometric variations that are possible e.g. change of the angle of inclination of trench/injection hole, increase in

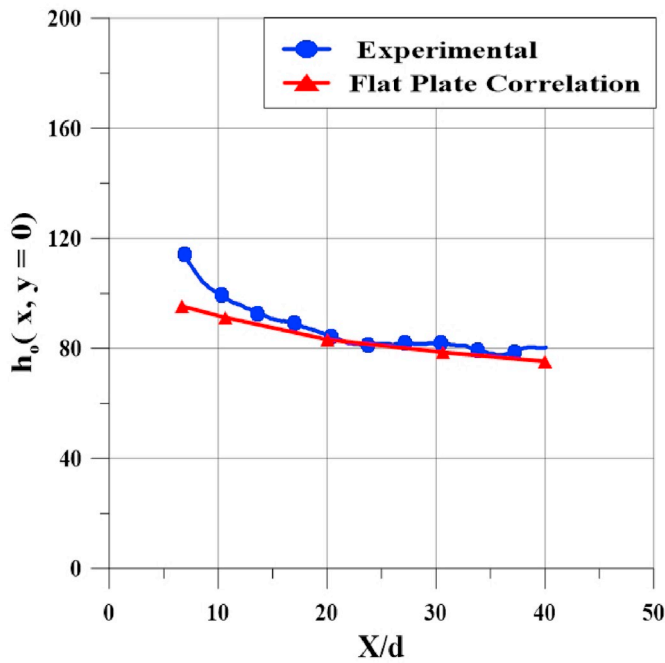


Fig. 8. Variation of $h_0(x, y = 0)$ when trench was covered (correlation: [23]).

the depth of the trench to a value larger than the hole diameter, provision for an additional diffusion angle to the trench in the direction of the mainstream etc. but in this investigation only one basic configuration was studied to examine its performance. The thickness of the injection plate was kept equal to $3d$ since this is the commonly used thickness in most studies. The length to diameter ratio of the holes therefore got fixed at 1.8. A shorter length to diameter ratio was not studied but a longer one equal to 5.5 was studied by extending the injection hole at inlet by gluing suitable diameter tubes to injection plate instead of increasing the plate thickness. A total of seven coolant injection holes were used to inject secondary fluid into the trench for the pitch to diameter ratio P/d equal to 3 case. The P/d equal to 6 case was obtained by blocking alternate holes but a new plate was fabricated for the P/d equal to 4.5 case.

The ejected fluid from the holes gets redistributed in the trench and the identity of the holes is not very distinct in the downstream direction. However, for plotting purposes a centerline is defined which is considered to be the geometric downstream direction along the center of the injection tube exit ($Y/d = 0$) as shown in Fig. 2(a). The smallest distance at which the measurements were made was $X/d = 7$. The isometric view of the inclined trench is shown in Fig. 2 (b) for better visualisation of the geometry. In Fig. 2 (c), the black coloured material is the base material and the purple is the thermal barrier coating. The machining of the base material is by using conventional milling and drilling. The barrier coating is put up by using a parallelepiped mask, which has a parallelogram cross-section. In addition, EDM can be also used to make such holes although the tooling has to be appropriately worked out.

The current geometry is different from those for which data is available in the literature and therefore two additional injection plates were fabricated to validate the experimental procedures used in the present investigation. The first is a geometry identical to that used by Eriksen and Goldstein [15], with jets entering the mainstream at an angle equal to 35° . The second is one of the several trench geometries reported by Lu et al. [2]. The geometry with trench width equal to $2d$, trench depth equal to $0.75d$ and hole to hole spacing equal to $3d$ was chosen and a schematic is shown in Fig. 2(d)

The details of experimental setup are given in Table 1.

3. Calculation methodologies

The heat supplied to the stainless steel foil-wall was calculated by taking the product of the voltage (V) across the foil ends and the current (I) flowing through the foil-wall. The blackened face of the stainless steel foil was exposed to the ambient and lost heat to the surroundings whereas the other face gave heat to the flow within the test section. The heat transferred to the flow within the test section was calculated as the difference between the electrical heat input and the heat loss (q_{loss}) from the surface of the foil exposed to the ambient.

The heat loss (q_{loss}) was experimentally determined by heating the foil-wall to different temperatures by applying a small heat flux and insulating the shiny side of the foil (which was exposed to the mainstream and film flows during experimentation) and recording the steady state temperature from the blackened side. The electrical heat input was therefore the heat lost to the ambient by the foil-wall. The temperature of the plate was measured for different heat loss and the heat loss as a function of the temperature difference between the foil-wall and ambient was plotted and used to correct the heat flux. This total loss has both the convective and radiative components of the heat loss. The radiative component was evaluated using $q = \epsilon \sigma (T(x, y)^4 - T_{amb}^4)$ and the convective part was obtained by subtracting this part from the total measured loss. The convective heat loss was plotted as a function of the temperature difference between the wall and ambient to obtain the loss calibration curve. The local foil-wall temperature measurements were used to compute and add the two loss components to obtain the total loss. The foil-wall temperature is however, non-uniform in the vertical direction and an average temperature was used to evaluate the convective component. The maximum non-uniformity in the measured temperature was 10°C at any given axial location and this value is accounted for in the calculation of the total uncertainty in the heat transfer coefficient and adiabatic wall temperature.

The methodology suggested by Fenot et al. [16] was used to obtain the adiabatic wall temperature and heat transfer coefficient at each location on the foil-wall by plotting the wall temperature for different heat flux values. The following expressions were used to extract the heat transfer coefficient and the adiabatic wall temperature:

$$q(x, y) = \frac{V \cdot I}{A} - q_{loss}(x, y) \quad (1)$$

$$\frac{q(x, y)}{h(x, y)} = T_w(x, y) - T_{aw}(x, y) \quad (2)$$

The heat transfer coefficient and adiabatic wall temperature in equation (2) are constant but are unknown and therefore at least two different measurements are required. Measurements of the foil-wall temperature were therefore obtained at five different foil-wall heat flux values with all other fluid dynamic parameters maintained same. The measured temperature at each location was plotted as a function of the net heat flux input to the flow. A straight line was fit through the data points using the minimization of sum of square of errors methodology. The slope of the line so obtained and its intersection point on the abscissa, gave the heat transfer coefficient the adiabatic wall temperature respectively as indicated by equation (2). A typical plot is shown in Fig. 3 and the linear relationship was observed at all locations.

The maximum temperature drop across the thickness of the foil wall was calculated to be less than 0.02°C using a one dimensional analysis in the thickness direction in the presence of heat generation. The temperature difference between the surface experiencing the flow and the opposite surface was therefore considered to be negligible.

The local effectiveness values were obtained from the adiabatic wall temperature measurements and the spanwise averaged effectiveness and heat transfer coefficient values were obtained from the local values by using the following expressions:

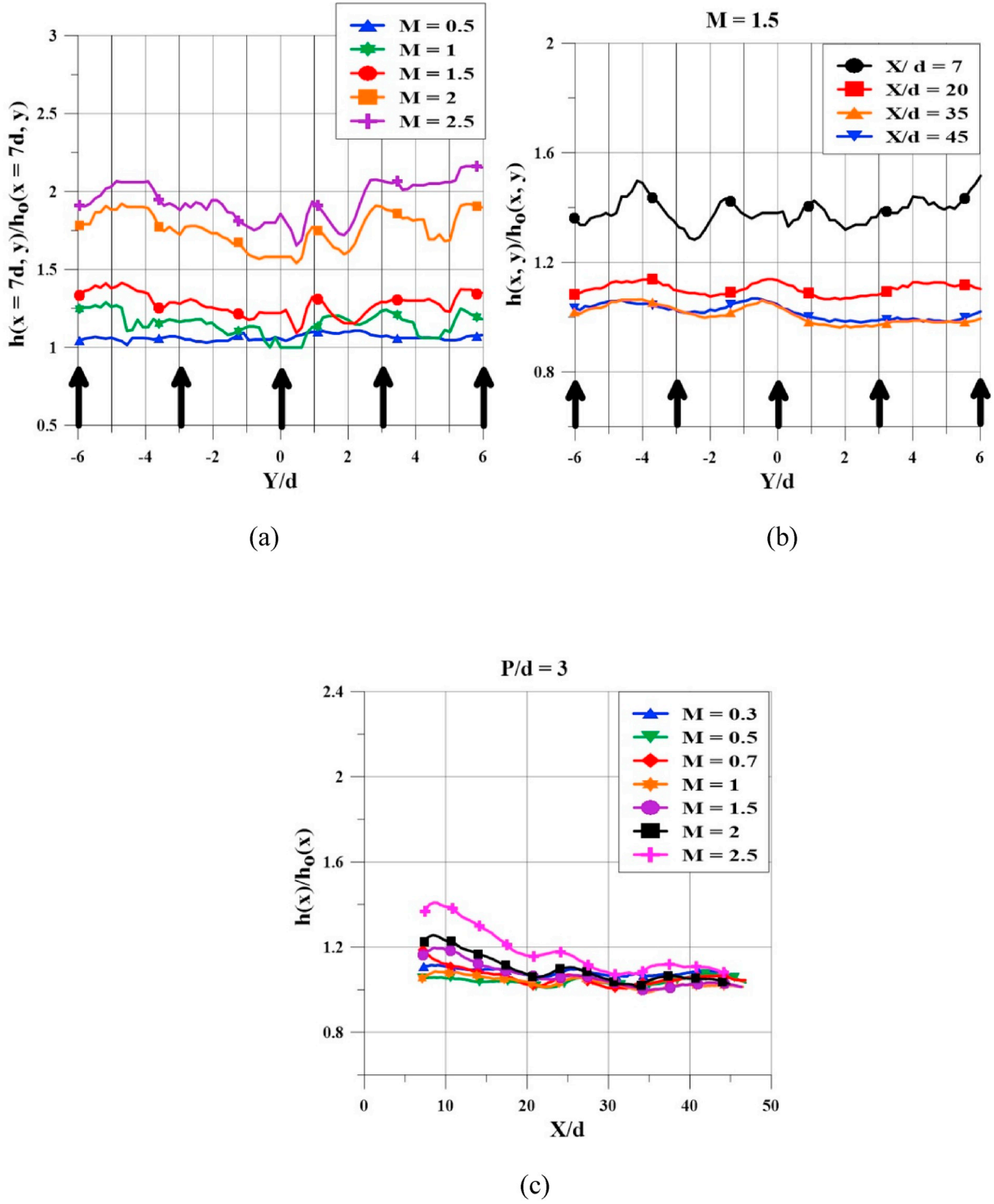


Fig. 9. Distribution of (a) Spanwise local $h(x = 7d, y)/h_0(x = 7d, y)$ for different M , (b) Spanwise local $h(x, y)/h_0(x, y)$ for different X/d for $M = 1.5$ and (c) Spanwise averaged $h(x)/h_0(x)$ for different M .

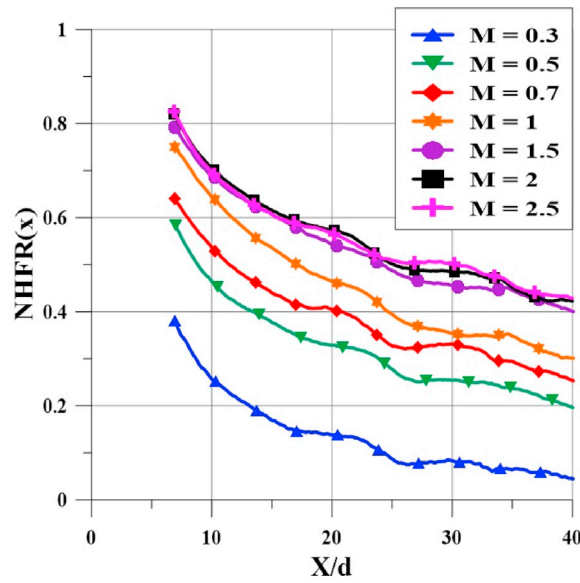
$$\eta(x, y) = \frac{[T_{aw}(x, y) - T_{\infty}]}{[T_j - T_{\infty}]}; \quad \eta(x) = \int_{-y}^y \eta(x, y) dy; \quad h(x) = \int_{-y}^y h(x, y) dy \quad (3)$$

The ratio of heat flux reduction in the presence of film cooling and the heat flux in the absence of film cooling is often termed as the Net Heat Flux Reduction ratio (NHFR) as reported by Sen et al. [17]. The NHFR represents combine effect of effectiveness and heat transfer coefficient. The effectiveness and heat transfer coefficient are together required to evaluate the film cooling performance and a higher NHFR is

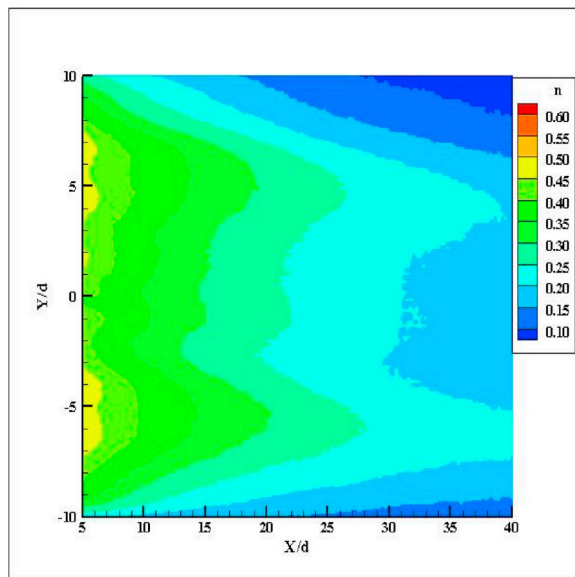
indicative of better film cooling performance. The NHFR is given as

$$\begin{aligned} NHFR(x, y) &= \frac{[q_0(x, y) - q_f(x, y)]}{q_0(x, y)} = 1 - \frac{h(x, y)[T_w(x, y) - T_{aw}(x, y)]}{h_0(x, y)[T_w(x, y) - T_{\infty}]} \\ &= 1 - \frac{h(x, y)}{h_0(x, y)} \left[1 - \frac{\eta(x, y)}{\phi} \right]; \quad \phi = \frac{[T_w(x, y) - T_{\infty}]}{[T_j - T_{\infty}]} \end{aligned} \quad (4)$$

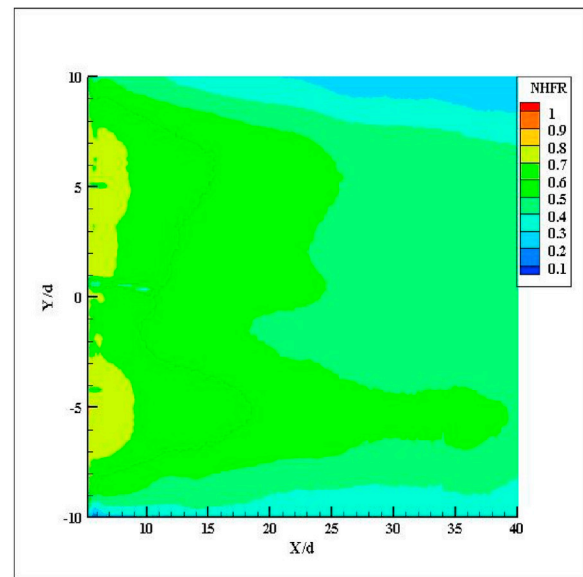
In the above equation for NHFR the overall cooling effectiveness (ϕ) for typical engine conditions is taken equal to 0.6 [2].



(a)



(b)



(c)

Fig. 10. (a) Distribution of (a) NHFR (x) for different blowing ratio M (b) Contours of η (x, y) for M = 1 and (c) Contours of NHFR (x, y) for M = 1.

The calibration curves for the thermocouples were obtained in-house and the uncertainty in temperature measurements of mainstream and secondary air was established to be 0.5°C . An infrared (IR) thermal camera (Mikron make M7600PRO) was used for the measurement of temperature of the foil-wall. The camera provides the option of using an operating temperature range of -40°C to 120°C and 0 – 500°C and the lower scale was used for all the measurements made in the current study. The accuracy of the camera is $\pm 2\%$ or 2°C of the reading but an independent calibration exercise was performed to obtain the uncertainty in measurement. The thermal camera was calibrated using a copper block which was painted with the same black paint that was used on the steel

foil that formed part of the test section. The copper block had three calibrated thermocouples embedded in it which were used to measure the temperature. The calibration curve was used to calculate the uncertainty to be 1.1°C for wall temperature measurements using the thermal camera. The DPT was calibrated using a water manometer and the uncertainty was calculated to be 0.1 mbar . All uncertainties in the above basic measured quantities were obtained with a 99.7% confidence level. The uncertainty in voltage and current measurements was taken to be equal to the least count of the measuring instruments i.e. 0.01 V and 0.1 A respectively. The uncertainties in the mass flow rate, heat transfer coefficient, effectiveness and NHFR were estimated to be 2%, 7.1%,

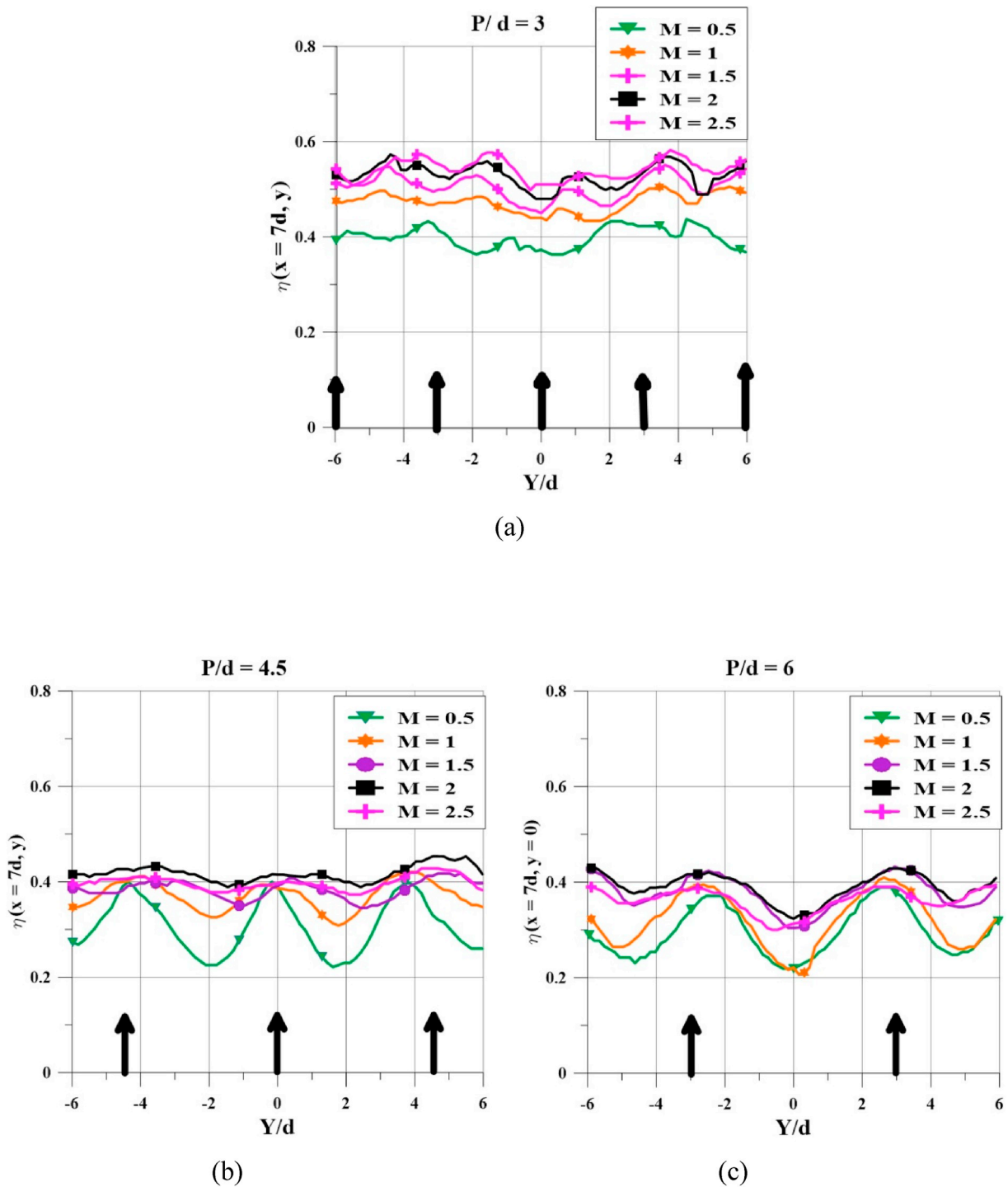


Fig. 11. Variation of $\eta(x/d = 7, y)$ for (a) $P/d = 3$, (b) $P/d = 4.5$ and (c) $P/d = 6$.

8.4% and 11.8%, respectively. The minimization of the least square error methodology was used to obtain the slope and intercept from the measured data. The methodology outlined by Young [18] was used to compute the variance of the slope and intercept. The uncertainty in the calculation of heat transfer coefficient and the adiabatic wall temperature are computed as the square root of the computed variance.

4. Results and discussions

The results from the current investigation are first compared with available data to gain confidence in the measurement procedures and

calculation methodologies. The detailed results are then presented followed by a comparison of the results of the current configuration with existing configurations that are known to provide good film cooling performance.

4.1. Validation of experimental setup

Fig. 4 (a) shows a comparison of the distribution of centerline effectiveness for film cooling over a flat plate with 35° simple hole injection of the present study with that reported by Godstein and Eckert, [19]; Jung and Lee [20]; Lutum and Johnson [21] and Singh et al. [22].

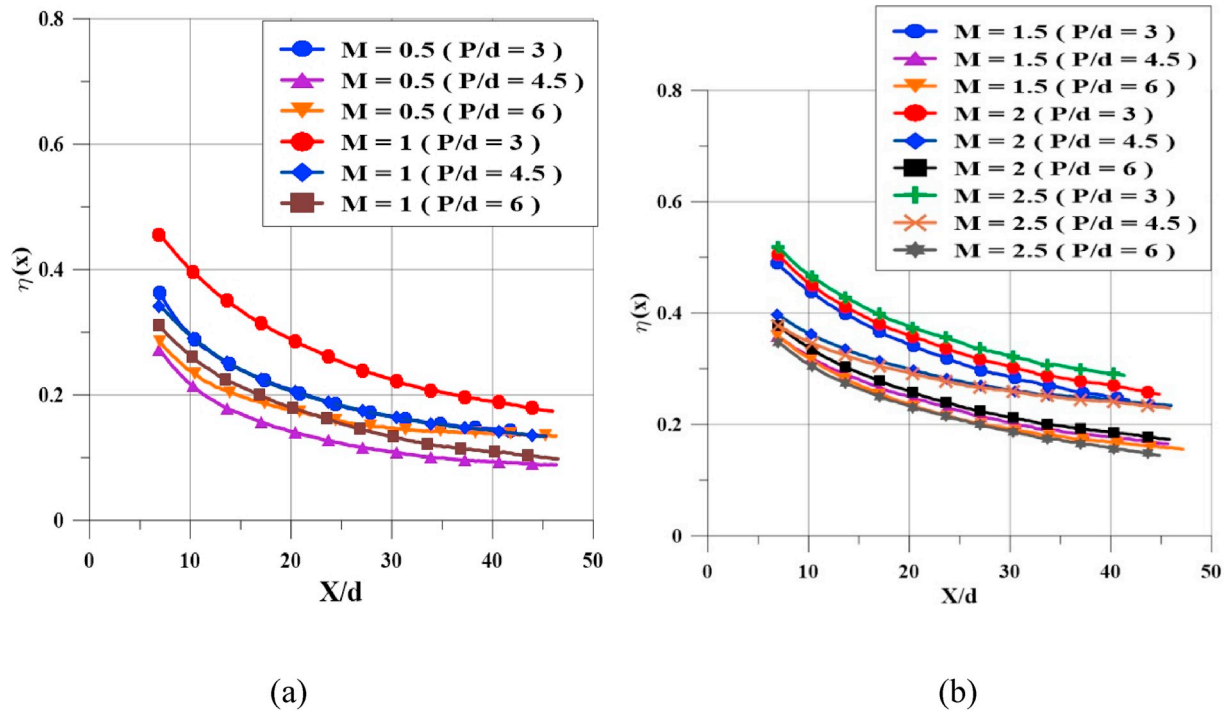


Fig. 12. Distribution of averaged effectiveness for P/d of 3, 4.5 and 6: (a) $M = 0.5$ and 1, (b) $M = 1.5$, 2 and 2.5.

The results of the present study are noticed to match reasonably well with these results. Fig. 4 (b) shows a comparison of the ratio of heat transfer coefficient with and without film cooling [$h(x, y)/h_0(x, y)$] for the above geometry with results reported by Eriksen and Goldstein [15] and the results are found to match within the limits of uncertainty. Fig. 5 shows the comparison of the spanwise averaged effectiveness values for the trench geometry with perpendicular walls for which data has been reported by Khalatov et al. [3] and Lu et al. [2] and a good agreement can be observed. The methodologies used in the present investigation for measurement of local and averaged effectiveness and heat transfer coefficient were therefore assumed to have been validated for use in the proposed geometry using the inclined trench.

4.2. Effectiveness and heat transfer coefficient distribution at different blowing ratio

Initial experiments were performed with the injection hole-to-hole spacing fixed at $P/d = 3$ with length to diameter ratio (L/d) = 1.8 after which the influence of varying P/d and L/d were studied.

The spanwise variation in effectiveness is usually expected to be high close to the injection location since the jet spread is minimum here. However, the trench assists in spreading the jet within it, and helps to reduce the spanwise variations prior to the fluid exiting into the mainstream and therefore variation here also is small. The variation at $X/d = 7$, which was the smallest distance at which the measurements were made and where the variation is likely to be maximum for all blowing ratios, is shown in Fig. 6 (a). The black arrows on the figure indicate the location of the jets. The variation is noticed to be minimal even for the largest blowing ratio used in the current investigation. Increase in blowing ratio can be noticed to increase the effectiveness values. The injection jets strike on the inclined wall and spread inside the trench and are likely to exit in the form of a slot jet with a varying degree of uniformity in the spanwise direction depending on the spacing between the jets and the blowing ratio. The spread of the fluid in the trench is good at all blowing ratios. Higher effectiveness values are observed at larger blowing ratios due to higher equivalent momentum of the fluid ejecting from the angular slot which is still small enough for the mainstream to

bend towards the surface. The vortex structure that would normally form as the mainstream rolls over the injected jets in the downstream region are dissipated as the jets strike the inclined wall. These weakened structures cause the spanwise variations that are observed in effectiveness and heat transfer coefficient values.

The distribution of spanwise effectiveness is shown in Fig. 6(b) for $M = 1.5$ for different axial locations and the spanwise variation as well as the magnitude can be noticed to be diminish at larger axial distances due to the mixing between the jet and mainstream fluids.

Fig. 7(a) shows the variation of centerline effectiveness ($Y/d = 0$) with increasing blowing ratio from 0.3 to 2.5. The spanwise averaged effectiveness is shown in Fig. 7(b) and it can be noticed to follow a very similar qualitative and quantitative trend as the local centerline variation. The very small variation of the effectiveness values in the spanwise direction causes the spanwise averaged effectiveness to be almost same in magnitude to the local centerline values. The reducing effectiveness with increasing distance in the downstream direction is due to increased mixing of the injected and mainstream fluids as observed for all other film cooling geometries. The rate of increase of effectiveness beyond $M = 1.5$ slows down as the effective momentum of the injected stream increases and the ability of the mainstream to bend it towards the surface reduces.

The heat transfer coefficients in the presence of film cooling were compared with those existing in the absence of film cooling. Measurements were made using the same injection plate with a thin tape stretched and glued firmly over the trench to obtain a smooth surface. Fig. 8 shows the variation of the heat transfer coefficients as a function of the downstream distance. The variation was negligible in the spanwise direction and only the variation along the streamwise centerline direction ($Y/d = 0$) is shown. The hydrodynamic boundary layer starts developing at the location where the constant cross section starts in Fig. 1 and the thermal boundary layer starts at the beginning of the heated foil-wall. The relationship for heat transfer downstream of an unheated starting length reported in Kays and Crawford [23] is also plotted on the figure. The experimental values were used for presenting the results in the non-dimensional form.

Fig. 9 (a) and (b) shows the spanwise variation of the heat transfer

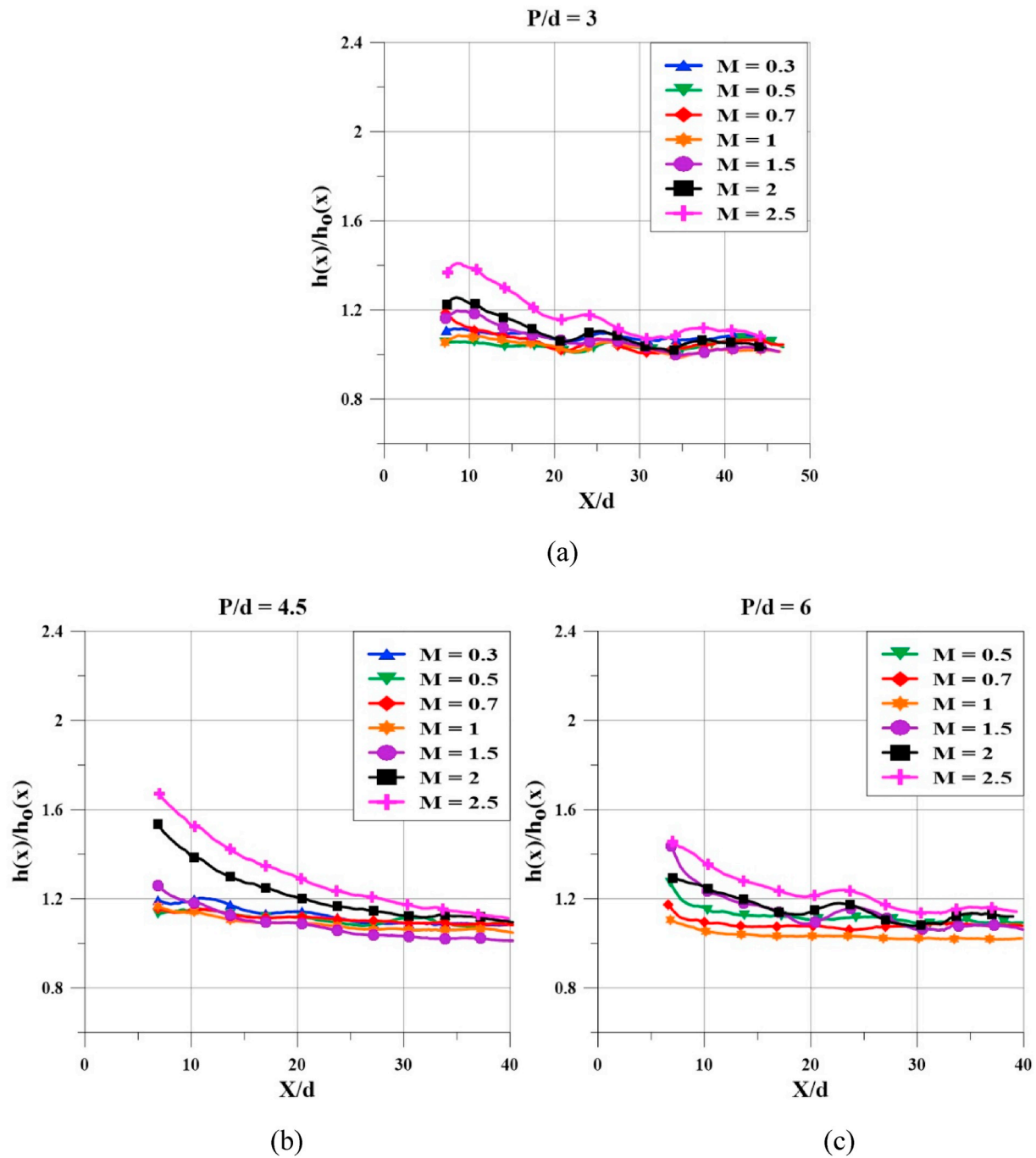


Fig. 13. Distribution of $h(x)/h_0(x)$ for (a) $P/d = 3$, (b) $P/d = 4.5$ and (c) $P/d = 6$.

coefficient ratio at $x/d = 7$, for several blowing ratios and at several X/d locations for $M = 1.5$, respectively. The values are observed to be nearly constant along the spanwise direction for all the blowing ratios and for all X/d at $M = 1.5$. The nearly uniform exiting ejected fluid stream weakens the mainstream flow tending to move towards the surface resulting in very little variation in the heat transfer coefficients in the spanwise direction. The edge regions (large Y/d locations) experience interaction with the mainstream at the sides also and result in slightly higher heat transfer coefficients and this effect is more prominent for higher blowing ratios at low X/d values. Fig. 9(c) shows the variation of the spanwise averaged heat transfer coefficient data as a function of downstream distance and the local variations which are almost similar to this are not plotted here. The heat transfer coefficient ratio is noticed to increase continuously as blowing ratio increases,

caused by the flow disturbance due to the increased penetration and interaction between injected fluid with different momentum flux values and the mainstream. The largest values of the heat transfer coefficients are noticed close to the injection location since the interaction between the jets and mainstream fluids is largest here. The rise in the heat transfer coefficients is moderate till $M = 1$ but after that the rise is rapid due to the increased penetration of the film into the mainstream. The reduction in the increase in effectiveness observed earlier also occurred at about this blowing ratio due to the same reason. The generally observed trend of the heat transfer coefficient ratio tending towards unity as the film loses its identity for large downstream locations from the injection zone is observed here also.

The variation of the spanwise averaged Net Heat Flux Reduction ratio $NHFR(x)$ with varying downstream distance is shown in Fig. 10 (a).

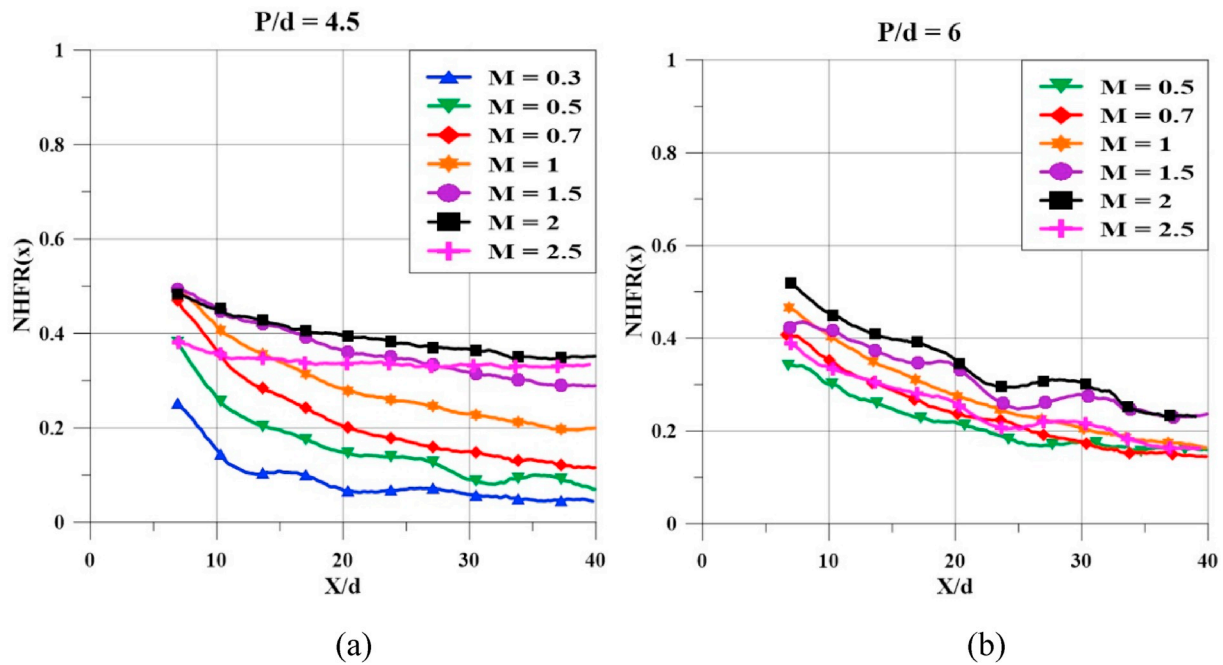


Fig. 14. Distribution of NHFR(x) for (a) $P/d = 4.5$ and (b) $P/d = 6$ for different M .

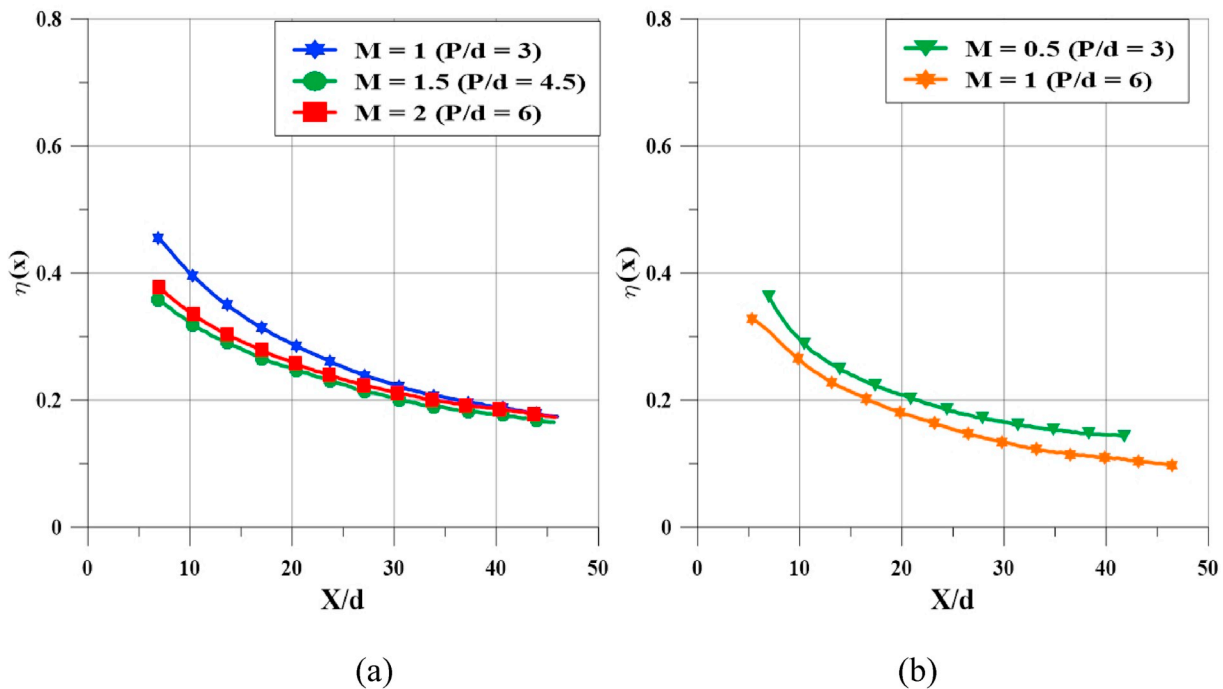


Fig. 15. Distribution of (a) $\eta(x)$ for $M = 1$ ($P/d = 3$), $M = 1.5$ ($P/d = 4.5$) and $M = 2$ ($P/d = 6$) and (b) $\eta(x)$ for $M = 0.5$ ($P/d = 3$) and $M = 1$ ($P/d = 6$) at constant mass flow rate.

The NHFR(x) is noticed to progressively increase from lower to higher blowing ratios with the increase becoming marginal after $M = 1.5$. The increased penetration of the secondary fluid into the mainstream at high blowing ratios causes the effectiveness values to drop. In addition, the heat transfer coefficient values rise rapidly due to stronger interaction of the injected fluid with the mainstream resulting in a reduction in the rise of NHFR values. The NHFR values can therefore be expected to fall at blowing ratios higher than those that were investigated in the current investigation (i.e. $M = 2.5$). A desirable feature of the present configuration that can be noticed is the high value of NHFR even for relatively

large values of downstream distance values. Fig. 10 (b) and (c) shows contours of effectiveness, and Net heat flux reduction for the blowing ratio equal to 1 and P/d equal to 3.

4.3. Effects of pitch to diameter ratio variation

The pitch to diameter ratio between the holes can alter the local and spanwise averaged distribution of effectiveness and heat transfer coefficient. Fig. 11 (a) and (b) shows spanwise distribution of effectiveness for $P/d = 4.5$ and the variation in the spanwise direction can be noticed

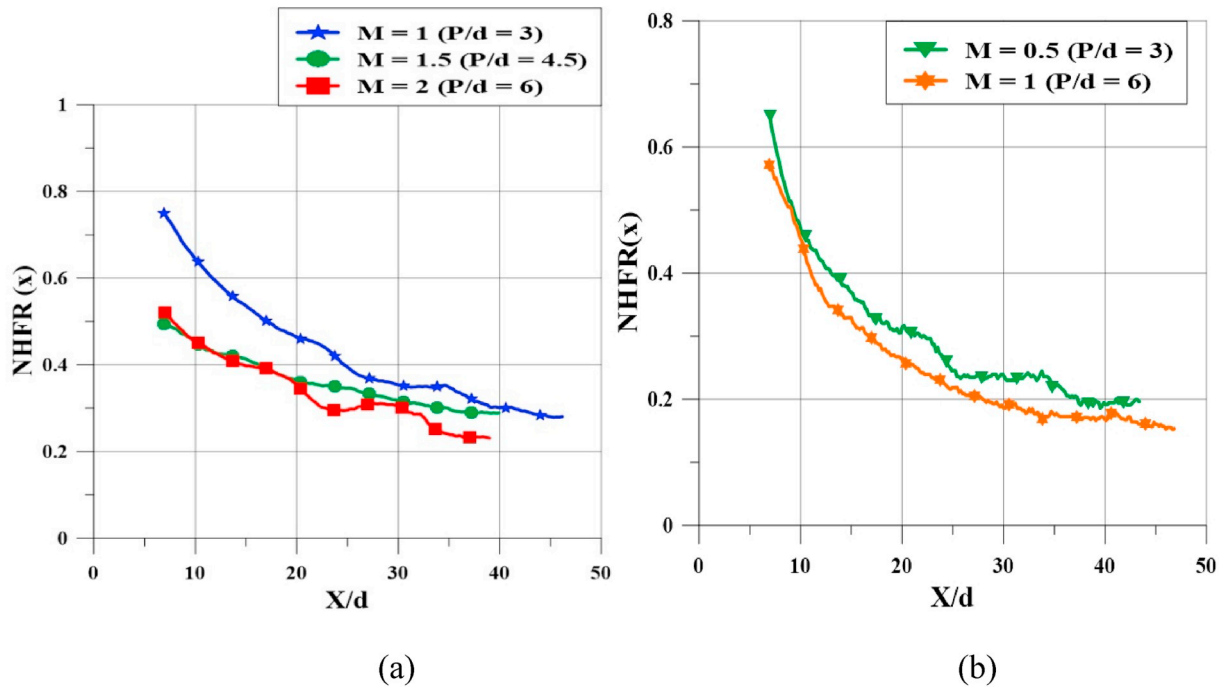


Fig. 16. Distribution of (a) NHFR (x) for $M = 1$ ($P/d = 3$), $M = 1.5$ ($P/d = 4.5$) and $M = 2$ ($P/d = 6$) and (b) NHFR (x) for $M = 0.5$ ($P/d = 3$) and $M = 1$ ($P/d = 6$) at constant mass flow rate.

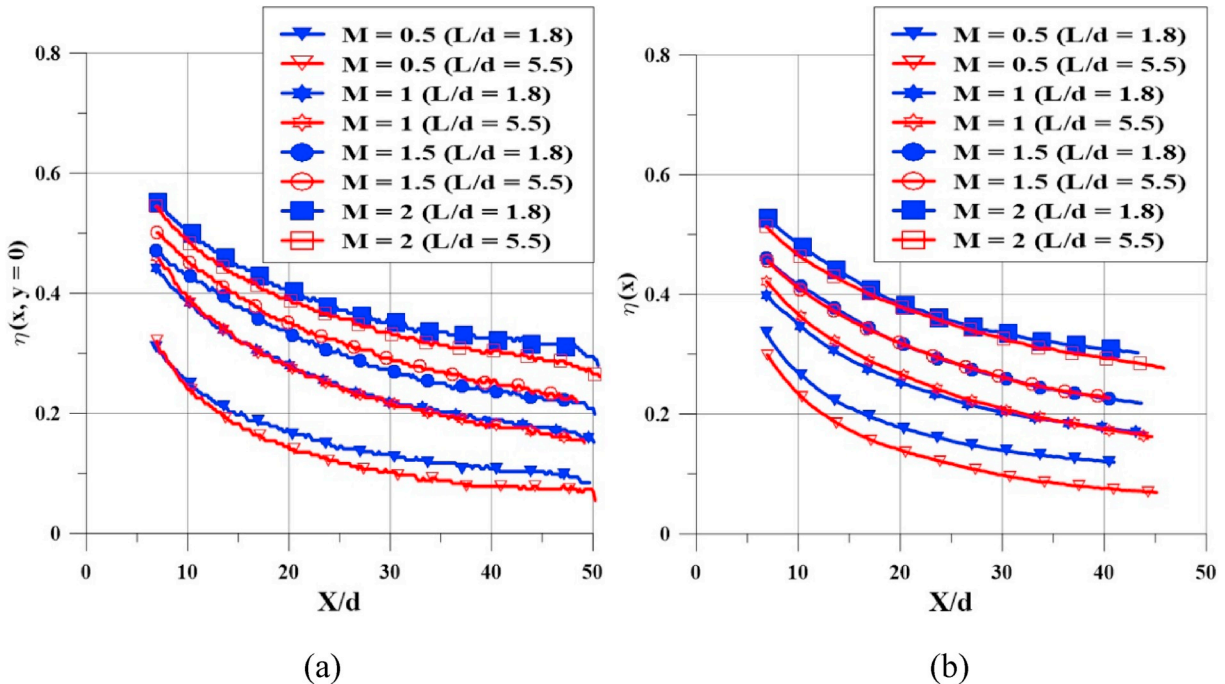


Fig. 17. Comparison of (a) $\eta(x, y = 0)$ and $\eta(x)$ for $L/d = 1.8$ and $L/d = 5.5$ for $M = 0.5, 1, 1.5$ and 2 .

to become larger at low blowing ratios compared to the $P/d = 3$ case. However, with increase in blowing ratios the spanwise variation is noticed to reduce significantly. At low blowing ratios since the mass flow injected is smaller with respect to the $P/d = 3$ case the spread within the trench is smaller which results in larger spanwise variations. However with increase in blowing ratios the spread is more and the increased interaction between adjacent jets within the trench leads to smaller variations. Fig. 11(c) shows the spanwise variations with an even higher $P/d = 6$ and the variations are now higher for higher blowing ratios. At

large blowing ratios, the interaction between the adjacent jets is reduced which weakens the uniformity of the exiting stream and the mainstream is able to penetrate more towards the surface causing larger spanwise variation. The effectiveness values for both these larger P/d ratios can be noticed to increase up to $M = 2$ and then reduce for the $M = 2.5$ case even though the spanwise variation is still relatively small. The modest increase in effectiveness from $M = 2$ to $M = 2.5$ for the $P/d = 3$ case indicates that effectiveness may possibly reduce for this case also if higher blowing ratios had been used.

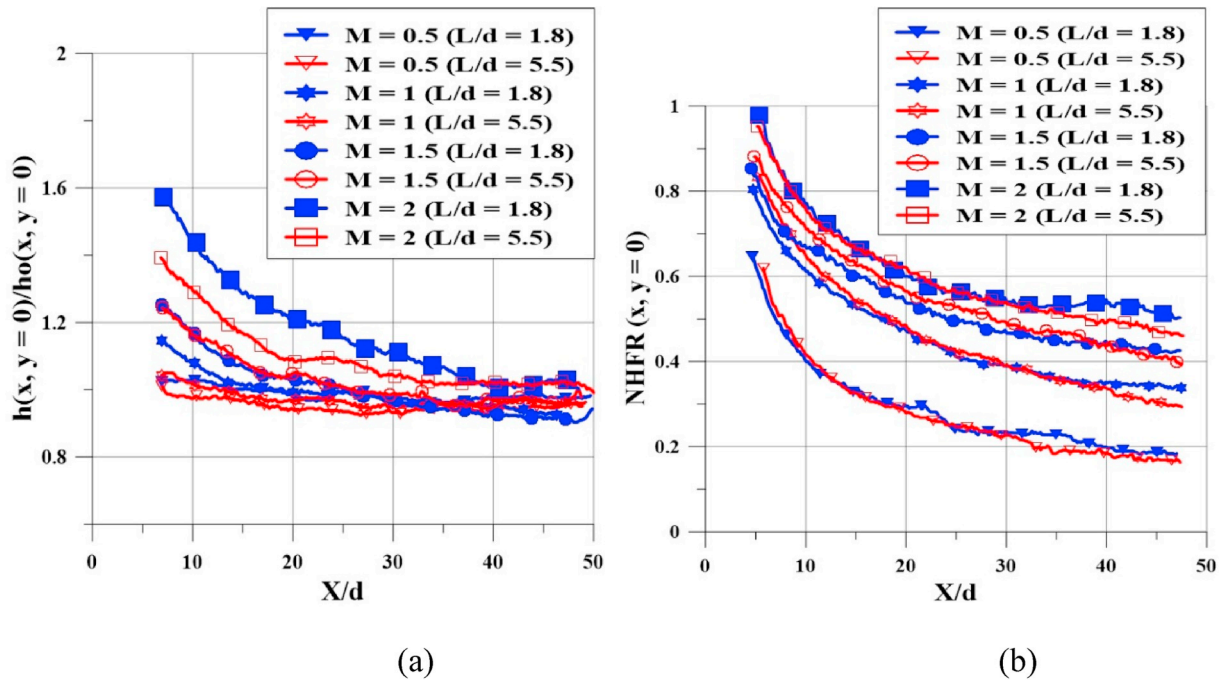


Fig. 18. Comparison of (a) $h(x, y = 0)/h_o(x, y = 0)$ and (b) NHFR (x, y) distribution for $L/d = 1.8$ and $L/d = 5.5$ for $M = 0.5, 1, 1.5$, and 2 .

Fig. 12 shows the variation of spanwise averaged effectiveness along the downstream direction for P/d values equal to 4.5 and 6 and the earlier data for $P/d = 3$ is also plotted on the same figure for the sake of comparison. The spanwise averaged effectiveness values are noticed to decrease with increasing P/d for identical blowing ratio values at all locations as expected. The film cooling effectiveness is reduced by 20%–30% for P/d of 6 compared to P/d of 3 but it must be noted that the mass flow rate is also smaller by 50%. The P/d equal to 3 gives better performance both in terms of better distribution of the coolant as well the magnitude of the effectiveness but at cost of increased mass flow rate.

Fig. 13 show the variation of the spanwise averaged heat transfer coefficient for P/d values equal to 3, 4.5 and 6. The variation can be noticed to be very small between the different P/d values at large X/d locations. At low P/d ratio, the injection stream exits as a nearly uniform jet and the mainstream experiences increased resistance for movement towards the surface resulting in low heat transfer coefficients. The injection stream is weaker in between the jets and mainstream moves towards the surface rather easily at very large P/d ratios resulting in large values of heat transfer coefficient. However at intermediate P/d ratios the mainstream accelerates towards the surface due to the smaller area of the relatively weak interaction region between the jets making the interaction with the surface more violent and therefore resulting in even higher heat transfer coefficient values. The heat transfer coefficient values for $P/d = 4.5$ are therefore noticed to be larger than the other two cases for a given blowing ratio. The stream wise distribution of spanwise averaged NHFR(x) for the $P/d = 4.5$ and 6 are shown in Fig. 14 and the values for the smaller P/d case can be noticed to be better than those for the larger P/d case. A comparison based on identical blowing ratio may not be a fair one for the three configurations since the mass flow rates are different.

Fig. 15 (a) shows the effectiveness distribution when the mass flow rate was maintained equal for the three P/d ratios investigated in the current study for high blowing ratios ($M = 1, 1.5$ and 2) whereas Fig. 15 (b) shows the effectiveness distribution for low blowing ratios ($M = 1, 0.5$). The averaged effectiveness values can be noticed to be nearly equal except close to the injection location for the high blowing ratio case. However, for the low blowing ratio case the effectiveness values are about 10% higher for lower P/d since at larger P/d values the

distribution in the trench is poorer. The values for P/d equal to 3 are found to be the highest for both cases and this may be considered to be superior compared to the other P/d ratios. The ratio of heat transfer coefficients are lower for the low P/d case due to the lower blowing ratio and therefore although the effectiveness values are very similar, the smaller heat transfer coefficient ratios result in higher NHFR values for this configuration as shown in Fig. 16 (a) and Fig. 16(b). The $P/d = 3$ case is again superior to the other two cases based on NHFR comparison.

4.4. Effects of length to diameter ratio variation

The development of the flow within the injection tube can affect the film cooling performance for jets directly entering the mainstream and length to diameter ratio is the main parameter that controls this. However, in the present situation, since the jets strike the inclined wall of the trench before spreading, the L/d ratio is not expected to affect the effectiveness or the heat transfer coefficient values. Nevertheless data was obtained for a larger value of $L/d = 5.5$ to observe any difference on the film cooling performance when this parameter is varied. In the experiment, L/d equal to 1.8 is obtained through thickness of the plate and L/d equal to 5.5 is obtained by extending holes in plenum chamber by sticking short tubes. Fig. 17 shows the variation of centerline effectiveness and spanwise averaged effectiveness as a function of downstream distance for different blowing ratios. The difference between the two different L/d values is less than 5% for $M > 1$. Fig. 18(a) shows the variation of the spanwise averaged heat transfer coefficient ratio [$h(x)/h_o(x)$] along the axial direction for L/d equal to 1.8 and 5.5 for different blowing ratios and the difference between the two cases is less than 10% with the change in L/d ratio. Fig. 18(b) shows the variation of NHFR with the variation in L/d and the differences can be observed to be very small. The difference in the heat flux reduction ratio can be assumed to be negligible over the range of L/d investigated in this study.

4.5. Comparison with other geometries

Fig. 19 shows a comparison of the spanwise averaged effectiveness for film cooling over a flat plate for the current configuration with trenches and other geometries which have been reported in the

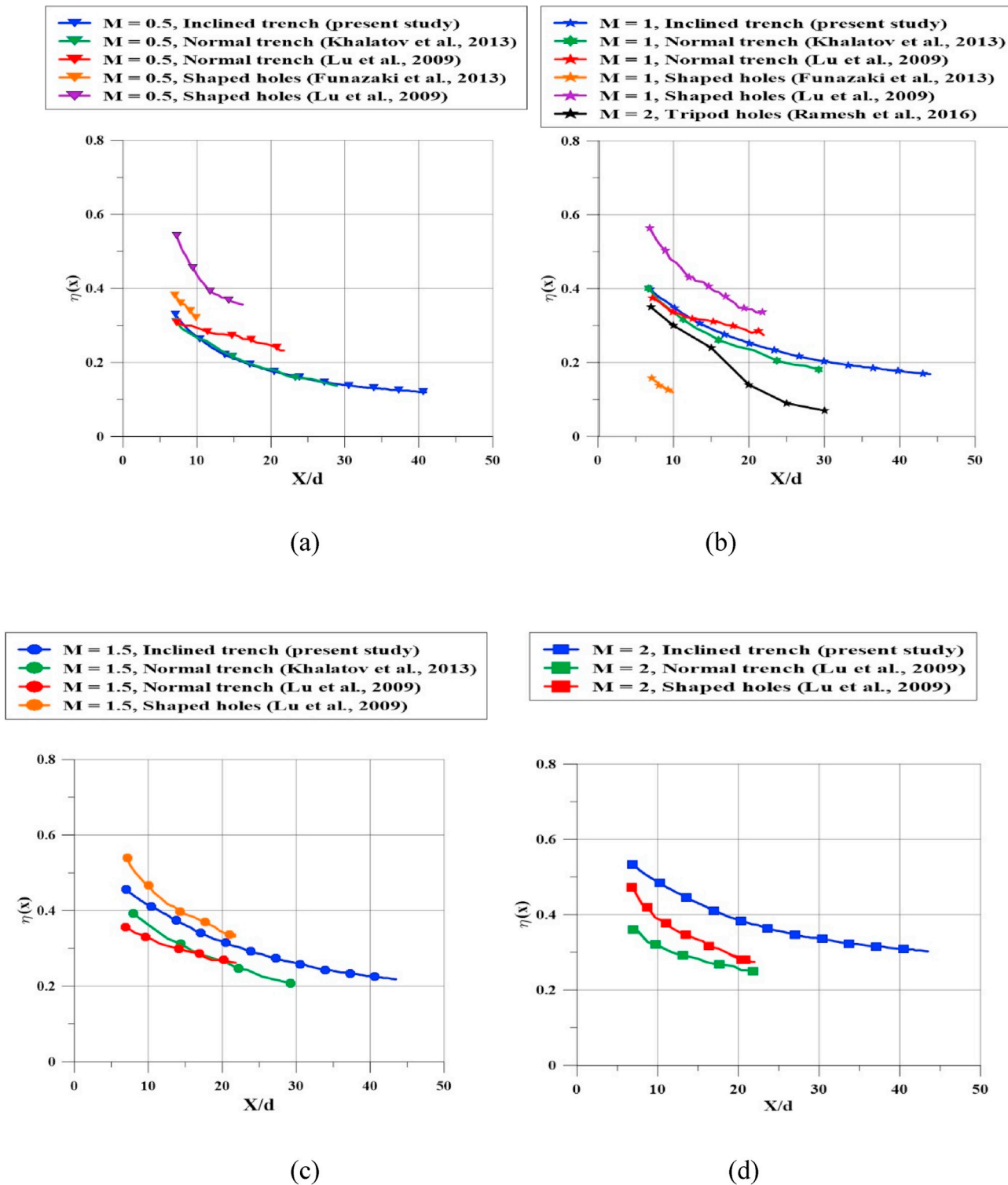


Fig. 19. Comparison of averaged effectiveness of inclined trench and geometries reported in literature for (a) $M = 0.5$, (b) $M = 1$, (c) $M = 1.5$ and (d) $M = 2$.

literature to perform very well. The shaped hole [2] with laidback angle of 15° which is reported to best performance for film cooling, to the best of our knowledge and the antivortex tripod holes are included in the comparison. The P/d is taken to be equal to 3 for all cases and while a comparison at equal blowing ratio is appropriate for all cases, antivortex hole comparison has to be at a blowing ratios must be double that for the other cases to keep the mass flow rate the same. It can be observed that for blowing ratios up to approximately 1.5 the shaped holes perform better than the other geometries. The injected fluid jet experiences lift

off for the shaped hole due to which its performance degrades at high blowing ratios. However, it must be noted that the spanwise variations are also likely to be higher for the shaped holes. The performance of the inclined trench is comparable to the normal trench till $M = 1.5$ but for higher blowing ratios the inclined trench can be observed to perform better. The comparison of averaged effectiveness of normal and inclined trench for blowing ratio equal to 1, 1.5 and 2 is shown in Fig. 20. Inclined trench performed better than normal trench for all blowing ratio.

A comparison of the results of heat transfer coefficient ratio $h(x)/$

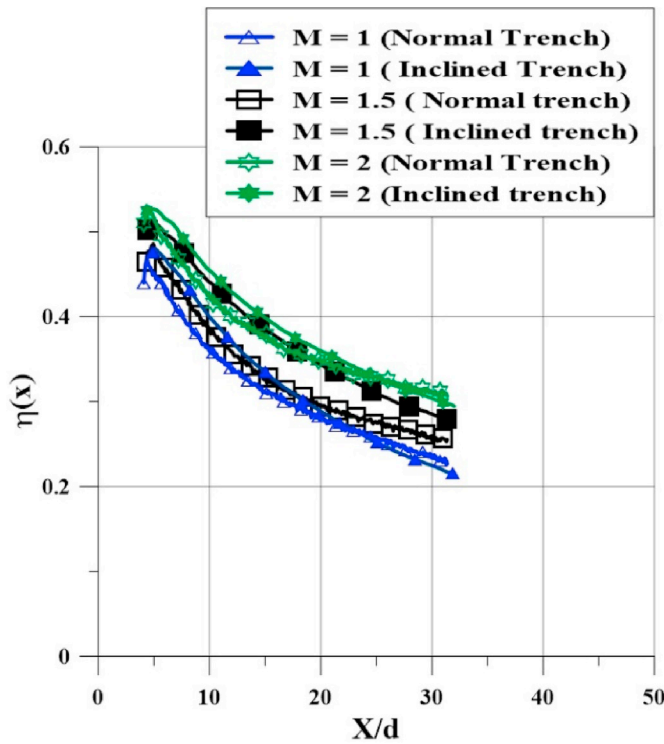


Fig. 20. Comparison of averaged effectiveness for normal trench and inclined trench.

$h_o(x)$ of shaped hole and normal trench reported by Lu et al. [2] and the present inclined trench is shown in Fig. 21 (a). The heat transfer coefficients of the shaped hole injection geometry and the normal trench configuration are noted to be higher for all X/d when compared to the values of the inclined trench. The secondary air jets strike on the inclined wall of trench for the present configuration and the ejected fluid is likely to come out at an angle to the surface smaller than that expected for the normal trench. This results in smaller penetration of secondary

air into the main stream due smaller effective momentum at exit in the direction perpendicular to the mainstream and smaller heat transfer coefficients are observed. The spanwise averaged NHFR calculated from the data reported for different configurations as well as for the current inclined trench is shown in Fig. 21 (b) and it can be noticed that the inclined trench performs very well here. The NHFR which is a combination of both the effectiveness and the heat transfer coefficient must be as high as possible. A high effectiveness and a low heat transfer coefficient are therefore desirable and the combined influence decides the performance of the configuration. The effectiveness for the inclined trench is smaller compared to the shaped holes for $M = 1$ and $M = 1.5$ but since the heat transfer coefficient is lower for the inclined trench, the two configurations perform equally well. However, at $M = 2$ the inclined trench combines the goodness of higher effectiveness and smaller heat transfer coefficients to perform much better than the other configurations. The inclined trench therefore has a better performance compared to the other geometries from the reduction in heat flux ratio perspective.

5. Conclusions

An inclined trench geometry with a row of injection holes has been proposed for film cooling of a flat surface for which local and spanwise averaged effectiveness and heat transfer coefficient data are presented. The spanwise variation in effectiveness and heat transfer coefficient is noticed to be very small. The spanwise averaged effectiveness values increase monotonically till about a blowing ratio equal to 2.5 for the $P/d = 3$ case, which was the highest value studied in the present investigation. The configurations with $P/d = 3, 4.5$ and 6 give almost the same effectiveness distribution when compared on an equal mass flow rate basis but since smaller heat transfer coefficients are obtained for the $P/d = 3$ configuration, the resulting NHFR is higher for the $P/d = 3$ case. Two values for the length to diameter ratio of the injection holes were studied and the differences in the results were insignificant which is in accordance with the expectation that the current configuration should be insensitive to length to diameter ratios. The Net Heat Flux Reduction for the proposed configuration is reasonably high (0.74–0.82 at $X/d = 7$ for variation of M from 0.5 to 2.5) and the reduction in the streamwise direction is relatively gradual making this a very competitive

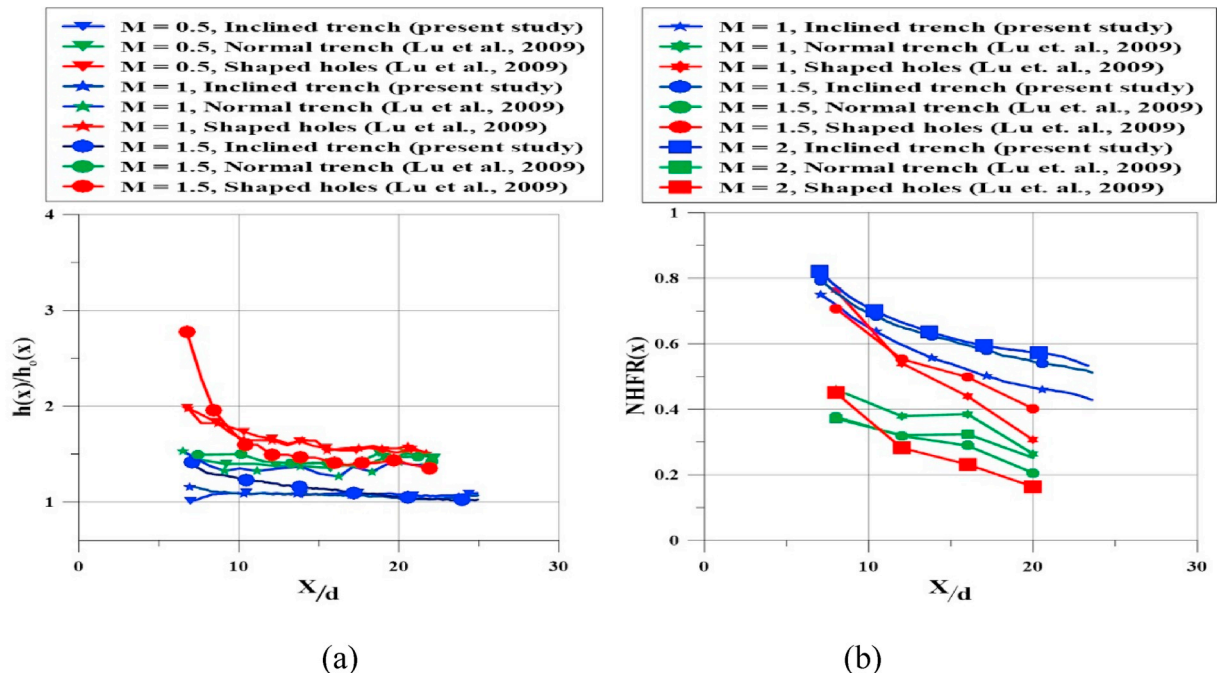


Fig. 21. Comparison of (a) $h(x)/h_o(x)$ and (b) $NHFR(x)$ of inclined trench and geometries reported in literature for $M = 0.5, 1, 1.5$ and 2 .

configuration with respect to the existing ones, which perform well.

The inclined trench provides good heat flux reduction values at high blowing ratio values ($M > 1$). Additional geometrical features, like varying inclination angle of trench, ratio of injection hole diameter to the trench impingement surface length etc., that were not included in the current study could be investigated to obtain an optimal configuration that could give better heat flux reduction values.

Appendix A. Supplementary data

Supplementary data to this article can be found online at <https://doi.org/10.1016/j.ijthermalsci.2019.106215>.

References

- [1] R.S. Bunker, A review of shaped hole turbine film cooling technology, *ASME J. Heat Transf.* 127 (2005) 441–453.
- [2] Y. Lu, A. Dhungel, S.V. Ekkad, R.S. Bunker, Effect of trench width and depth on film cooling from cylindrical holes embedded in trenches, *ASME J. Turbomach.* 131 (2009), 011003-1-13.
- [3] A.A. Khalatov, I.I. Borisov, Y.Y. Dashevskiy, Shevtsov S.V. Kovalenko, Flat plate film cooling from a single –row inclined holes embedded in a trench: effect of external turbulence and flow acceleration, 2013, *Thermophys. Aeromech.* 20 (6) (2013) 713–719 (FH).
- [4] L. Jia, R. Jing, J. Hongde, Film cooling performance of the embedded holes in trenches with compound angles, in: *Proceedings of ASME Turbo Expo 2010: Power for Land, Sea and Air GT2010*, Glasgow, UK, 2010.
- [5] H.A. Zuniga, J.S. Kapat, Effect of increasing pitch to diameter ratio on the film cooling effectiveness of shaped and cylindrical holes embedded in trenches, in: *Proceedings of ASME Turbo Expo 2009, GT2009*, Orlando, Florida, USA, 2009, pp. 1–10.
- [6] K. Lee, K. Kim, Film cooling performance of cylindrical holes embedded in a transverse trench, *Numer. Heat Transf. A* 65 (2014) 127–143.
- [7] A.M.M. Abdala, F.N.M. Elwekeel, Q. Zheng, Theoretical film cooling effectiveness investigation on C3X vane suction side with multi trench configuration, in: *Proceedings of 2012 International Conference on Mechanical Engineering and Material Science (MEMS 2012)*, 2012, pp. 171–174.
- [8] H.I. Oguntade, G.E. Andrews, A.D. Burns, D.B. Ingham, M. Pourkashanian, Improved trench film cooling with shaped trench outlets, *ASME J. Turbomach.* 135 (2013) 1–10, 021009.
- [9] W. Zhang, S. Zhou, Z. Wu, G. Li, Z. Kou, Film cooling mechanism of combined hole and saw-tooth slot, *Int. J. Turbo Jet Engines* (2017) 1–9.
- [10] E. Kianpour, N.A.C. Sidik, M.A. Wahid, Cylindrical and row trenched cooling holes with alignment angle of 90° , *CFD Lett.* 5 (4) (2013) 165–173.
- [11] M.A. Pakhomov, V.I. Terekhov, A.A. Khalatov, I.I. Borisov, Film cooling effectiveness with injection through circular holes embedded in A transverse trench, *Thermophys. Aeromech.* 22 (3) (2015) 329–338.
- [12] C. Wang, X. Sun, J. Zhang, Uncertainty analysis of trench film cooling on flat plate, *Appl. Therm. Eng.* 156 (2019) 562–575.
- [13] W. He, Q. Deng, W. Zhou, T. Tiejun Gao, Z. Feng, Film cooling and aerodynamic performances of a turbine nozzle guide vane with trenched cooling holes, *Appl. Therm. Eng.* 150 (2019) 150–163.
- [14] R.D. Mehta, P. Bradshaw, Design Rules for Small Low Speed Wind Tunnels, *The Aeronautical Journal of the Royal Aeronautical Society*, 1979, pp. 443–449.
- [15] V.L. Eriksen, R.J. Goldstein, Heat transfer and film cooling following injection through inclined circular tubes, *Trans. ASME J. Heat Transf.* (1974) 239–245.
- [16] M. Fenot, J.J. Vullierme, E. Dorignac, Local heat transfer due to several configurations of circular air jets impinging on a flat plate with and without semi-confinement, *Int. J. Therm. Sci.* 44 (2005) 665–675.
- [17] B. Sen, D.L. Schmid, D.G. Bogard, Film cooling with compound angle holes: heat transfer, *Trans. ASME J. Turbomach.* 118 (1996) 800–806.
- [18] H.D. Young, *Statistical Treatment of Experimental Data*, McGraw Hill Book Company, 1962.
- [19] R.J. Godstein, E.R.G. Eckert, Effects of hole geometry and density on three-dimensional film cooling, *Int. J. Heat Mass Transf.* 17 (1974) 595–607.
- [20] I.S. Jung, J.S. Lee, Effects of orientation angles on film cooling over a flat plate: boundary layer temperature distributions and adiabatic film cooling effectiveness, *J. Turbomach.* 122 (2000) 153–159.
- [21] E. Lutum, B.V. Johnson, Influence of the hole length to diameter ratio on film cooling with cylindrical holes, *ASME-J. Turbomach.* 121 (1999) 209–215.
- [22] K. Singh, B. Premachandran, M.R. Ravi, Experimental and numerical studies on film cooling with reverse/backward coolant injection, *Int. J. Therm. Sci.* 111 (2017) 390–408.
- [23] W.M. Kays, M.E. Crawford, *Convective Heat and Mass Transfer*, vol. 3, McGraw-Hill, Inc., Edition, 1993, pp. 255–304.